DOI: 10.13009/EUCASS2017-133



# Design and Experimental Evaluation of Liquid Oxidizer Injection System for Hybrid Rocket Motors

*Mohammed Bouziane*, Artur Elias de Morais Bertoldi**, Dahae Lee**, Praskovia Milova**, Patrick Hendrick** and Michel Lefebvre**

**Royal Military Academy*

*Avenue de la Renaissance30, 1000 Brussels, Belgium*

***Université Libre de Bruxelles*

*F.D. Roosevelt Avenue 50, 1050 Brussels, Belgium*

## Abstract

Liquid oxidizer injection systems play an important role in hybrid rocket motors. In most configurations, a liquid oxidizer is injected in the combustion chamber by means of an atomizer, and a spray is formed. The liquid oxidizer droplets vaporize in the pre-chamber and combustion port where they react with gaseous fuel originated from the solid grain surface. The characteristics of the liquid oxidizer spray have significant effects on the solid fuel regression rate, combustion stability and, thus, the overall propulsive system performance. The aim of this research is to study the impact of the injection system design on the characteristics of the oxidizer flow pattern, and to evaluate different injectors for future testing in firing conditions using paraffin fuel and $N_2O$ oxidizer. For this purpose, three types of injector plates were designed, manufactured and tested: hollow-cone, pressure swirl and vortex. The design was driven by the requirement of an oxidizer mass flow of 550 g/s. The tests were carried out in 'cold' conditions, first, with water, and then, with the oxidizer (nitrous oxide $N_2O$). The discharge coefficient of each type of injector plate was obtained. The main parameters of a spray such as spray semi-angle were measured using a high-speed camera, and the Sauter Mean Diameter (SMD) and droplet size distribution – using a laser scattering system. The flow patterns of each type were compared with the base-line showerhead injector used with the same mass flow rate. Based on the results of the current experimental investigation in 'cold' conditions, the evaluation of the three designs of a liquid oxidizer injection system was done in order to estimate the best fit for the firing tests using the 1 kN lab-scale hybrid rocket motor developed at Université Libre de Bruxelles (ULB).

## 1. Introduction

Recently there are more investigations about hybrid rocket propulsion, due its advantages over the other chemical propulsion systems, in particular the safety aspects and possibility to control the motor thrust. However, the main shortcoming of hybrid motor is the low regression rate of the solid fuel. In order to overcome it, a number of techniques have been proposed, as the use of metal powders in the solid fuel matrix or by changing the injector flow pattern. The liquid oxidizer injection system plays an important role in hybrid and liquid rocket engines and the atomization of a liquid propellant is most commonly carried out by injecting the oxidizer through one individual injector. Due to the importance of the atomization process on the combustion performances, the injection system design and its different configurations have been matter of study over the time.

One of the methods is to induce a rotational motion on the flow by the use of a vortex atomizer. Tests performed by Orbital Technologies Corporation (USA) suggest that using gaseous oxygen unique coaxial, co-swirling, counter flowing vortex pair, it is possible to induce higher solid fuel regression rates than the similar classical hybrid engines [1-4]. To generate this flow field, oxidizer is injected through a swirl injector located between the aft end of the fuel grain and the inlet of the convergent portion of the exit nozzle, that exhibit a significant increase in regression rate, around eight times larger than a conventional head end injected hybrid [1]. In the same period, Yuasa et al. tested also gaseous oxygen injected by vortex in the front head of the grain, achieving a regression rate three times faster than observed in the classical hybrid motors [5-8]. Bellomo et al. investigate liquid nitrous oxide injected in vortex configuration, an increase in the regression rate up to 51% has been measured and the instability in the combustion chamber is lower when compared with the vortex and axial injection [9-11]. Recently, Messineo et al. did a numerical comparison between swirl and axial injection to understand the effects of the swirl on the engine combustion efficiency and stability, and an experimental result showed that the regression rate rise by 40 % with swirl [12].

DOI: 10.13009/EUCASS2017-133



Another atomizer, simple to design and reliable, is the pressure swirl injector (PSW) and its application in hybrid rocket motors is relatively new. In the pressure-swirl atomizers the liquid is fed to the injector through tangential passages giving the liquid a high angular velocity, and forming, in the swirl chamber, a liquid layer with a free internal surface, thus creating a gas-core vortex. The liquid then is discharged from the nozzle in the form of a hollow conical sheet which breaks up into small droplets [13]. The main pressure swirl design parameters are the discharge coefficients, spray-cone angle, Sauter Mean Diameter (SMD). A. Lefebvre et al presented some predictions on discharge coefficients, spray-cone angles, and mean droplet sizes [14-17].
In this work four different injectors were designed, showerhead (SH), hollow-cone (HC), pressure-swirl (PSW) and vortex atomizer (VOR), and a series of cold flow test were carried out to perform their fully characterization. For this purpose, a new test bench was assembled in the Aero-Thermo-Mechanics Department equipped with a fast speed camera and a laser scattering system. Based on the results of the current experimental investigation in 'cold' conditions, the evaluation of the injector designs were done in order to estimate the best fit for the firing tests using the 1 kN lab-scale hybrid rocket motor developed at Université Libre de Bruxelles (ULB).

## 2. Injection system design

The new ULB hybrid rocket motor (ULBHRE) was developed to delivery 1 kN thrust, which is related with the total mass flow rate by the equation (1), where $F$ is the thrust, $I_{sp}$ is the specific impulse and $g_o$ is the standard acceleration of gravity. The total mass flow rate ($\dot{m}$) and the oxidizer mass flow rate ($\dot{m_{ox}}$) are related through equation (2). Equation (3) shows the main variables that influence the oxidizer mass flow rate, as the discharge coefficient ($C_d$), the number of individual injectors ($N_{inj}$), the area of the injector ($A_{inj}$), the oxidizer density ($\rho_{ox}$) and the pressure drop in the injector ($\Delta P$). The injectors were designed based on the theoretical parameters of the ULBHRE motor, table 1, with the goal to delivery 550 *g/s* based in an injector pressure drop of 25 bar.

$$F = \dot{m} \cdot I_{sp} \cdot g_o \tag{1}$$

$$\dot{m} = \dot{m_f} + \dot{m_{ox}} \tag{2}$$

$$\dot{m}_{ox} = C_d \cdot N_{inj} \cdot A_{inj} \cdot \sqrt{2 \cdot \rho_{ox} \cdot \Delta P} \tag{3}$$

Table 1: Theoretical parameters of the ULBHRE

| **Parameter** | | **Parameter** | |
|---|---|---|---|
| Oxidizer | $N_2O$ | Initial oxidizer to fuel ratio | ~ 7.9 |
| Fuel | Paraffin | Oxidizer mass flow rate (g/sec) | 550 |
| Nominal thrust (kN) | 1.0 | Average Fuel mass flow rate (g/sec) | 70 |
| Chamber pressure (bar) | 25 | Total mass flow rate (g/sec) | 620 |
| Nozzle expansion rate | 4 | Burn time (sec) | 10 |

### 2.1 Shower head injector (SH)

The 3D-model of each injector was done using the commercial software SolidWorks® and manufactured at ULB. The showerhead injector, illustrated in figure (1), has 11 orifices spread equally in two different radiuses and one element in the center in order to deliver a homogenous distribution of the oxidizer flow into the chamber.

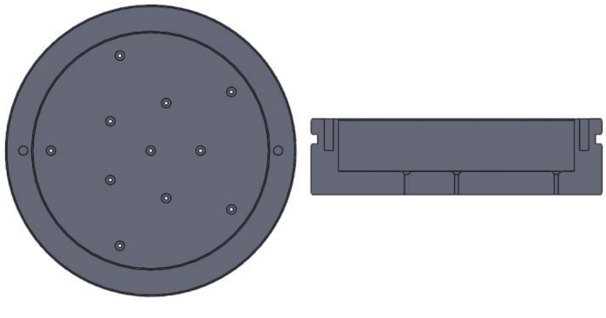

Figure 1: Shower head plate injector

DOI: 10.13009/EUCASS2017-133



## 2.2 Hollow-cone injector (HC)

Figure (2) shows the hollow-cone (HC) injector, with 11 individual elements also. Each injector is inclined at an angle of 15 degrees, in order to drive the flow into the wall of the inner fuel grain surface. When the jet collides with the grain, in two different regions, before the contact point and between jet core and the wall of pre-chamber, is created the recirculation zone. After this impingement point, a redevelopment zone started, within a boundary layer established and a diffusion flame is formed [18].

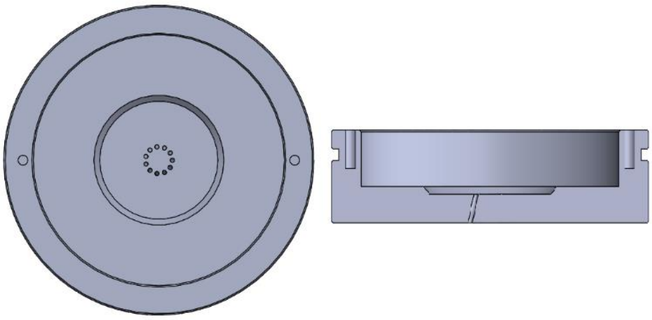

Figure 2: Hollow-cone plate injector

## 2.3 Pressure swirl injector (PSW)

The pressure-swirl injector (PSW) was designed as suggest by [13]. Figures (3) and (4) show the 2D drawing of PSW injector and the 3D design, respectively. The injector plate has 6 individual pressure-swirl elements with four tangential passages and its nozzle to set the oxidizer mass flow rate with the requirements of ULBHRE motor. In figure (3) is presented also the nomenclature of the PSW atomizer, as the nozzle discharge diameter ($D_0$) which must be chosen depending of the mass flow rate required, the nozzle length ($L_0$), the swirl chamber diameter ($D_s$), the swirl chamber length ($L_s$), the tangential entry passage diameter ($D_p$), the tangential entry passage length ($L_p$) and the air core diameter ($D_a$).

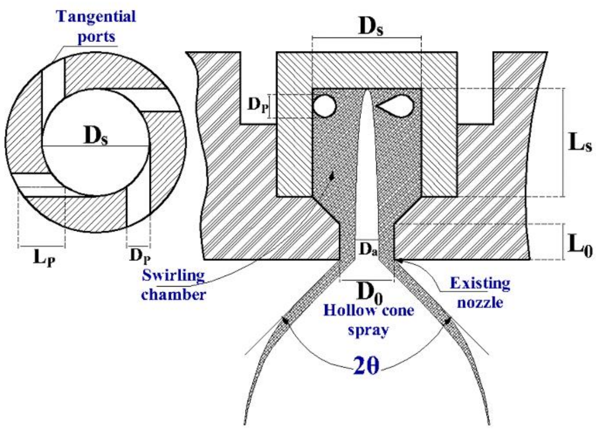


Figure 3: schematic of PSW injector

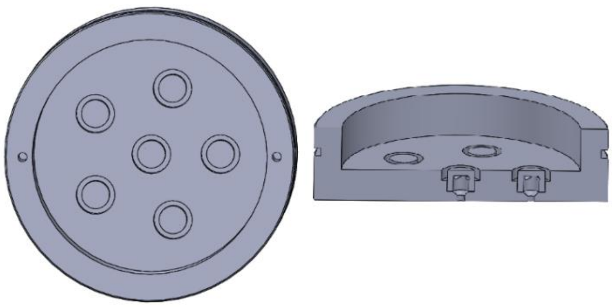

Figure 4: Pressure swirl plate injector assembled with the upper part of the nozzle

DOI: 10.13009/EUCASS2017-133



The flow number ($FN$) is calculated using the equation (4), where $\dot{m}_L$ is the liquid mass flow rate, $\rho_L$ is the liquid density and $\Delta P$ is the pressure drop. The ratio $L_s/D_s$ should be reduced to minimize wall friction losses. However, a limiting value is needed to achieve the liquid flow stabilization and the generation of a uniform vortex sheet. This ratio must be higher than 0.5, and a typical value recommended for appropriate design is 1.0 [19]. The parameter $L_0/D_0$ should also be reduced to minimize friction losses at the atomizer exit. As well as, the ratio $L_p/D_p$ should be bigger than 1.3, because a short tangential inlet passage channel may develop a diffuse discharge create an unstable spray [18]. Finally, one has to heed of the obvious limitations of the manufacturing process itself.
There are some empiric relations to predict the discharge coefficient $C_d$, they are given in equations (5) and (6) [14,20], where, $U_0$ (cm/s) is the velocity of the liquid at the atomizer tip and $\mu_L$ (cp) is the liquid dynamic viscosity. This coefficient is influenced mostly by set of parameters, that is $0.19 < \frac{A_p}{D_s \cdot D_0} < 1.21$ and $1.41 < \frac{D_s}{D_0} < 8.13$ [21], where $A_p$ is the tangential entry passage cross-sectional area.

$$FN = \frac{\dot{m}_L}{\sqrt{\rho_L \cdot \Delta P}} \tag{4}$$

$$C_d = 0.35 \cdot \left(\frac{D_s}{D_0}\right)^{0.5} \cdot \left(\frac{A_p}{D_s \cdot D_0}\right)^{0.25} \tag{5}$$

$$C_d = 0.45 \cdot \left(\frac{D_0 \cdot \rho_L \cdot U_0}{\mu_L}\right)^{-0.02} \cdot \left(\frac{L_0}{D_0}\right)^{-0.03} \cdot \left(\frac{L_s}{D_s}\right)^{0.05} \cdot \left(\frac{A_p}{D_s \cdot D_0}\right)^{0.52} \cdot \left(\frac{D_s}{D_0}\right)^{0.23} \tag{6}$$

The dimensions, in our design, were adjusted to simplify the atomizer construction, but respecting the dimensionless groups conditions described above. Table 2 shows the main dimensions of PSW.

Table 2: Main parameters of the PSW injector

| **Dimension** | **Value** | **Dimension** | **Value** |
|---|---|---|---|
| $D_0$ | 3 mm | $L_s$ | 6 mm |
| $L_0$ | 2 mm | $D_p$ | 1.3 mm |
| $D_s$ | 6 mm | $L_p$ | 2.58 mm |

## 2.4 Vortex injector (VOR)

Several configurations of vortex injector can be found in the technical literature, depending on the velocity components given to the flow at the inlet. In our case, the injector holes were ordered in combination between both axial and radial component, 45° each one, to distribute equally the flow towards the inner fuel grain surface. Figure (5) shows the VOR injector plate.

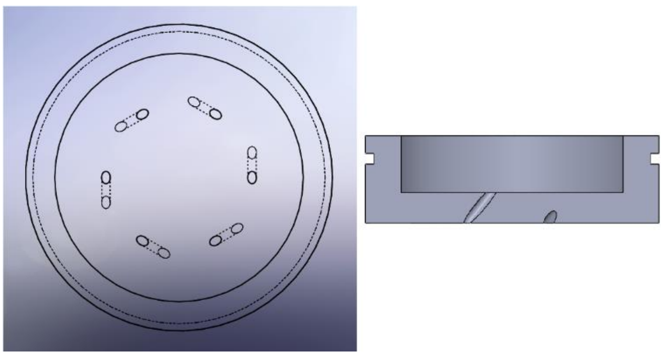

Figure 5: Vortex plate injector

DOI: 10.13009/EUCASS2017-133



## 3. Experimental setup

In order to characterize the injectors, a new test bench was developed in the Aero-Thermo-Mechanics Department at the ULB. The system was designed to maximize the number of the tests that can be performed and in interchangeable parts that allow us to use water and liquid Nitrous Oxide as duty fluid.
Figure (6) shows the schematic of the test bench. The regulator (R) control the Nitrogen pressure from 5 to 40 bar, a series of manual valves were used to control the pressure in different points of the system and to purge, when necessary. The flow is controlled by the use of the solenoid valve (MV) placed near the injector head-front to minimize the open-close delay time. The pressure upstream is obtained by the use of a pressure transducer, the temperature with a thermocouple type K and the downstream pressure is taken as 1 atm. The data acquisition system was the NI USB-6218 connects with the LabView interface. When Nitrous oxide is used, the water-bottle is changed and no pressurization system is required.

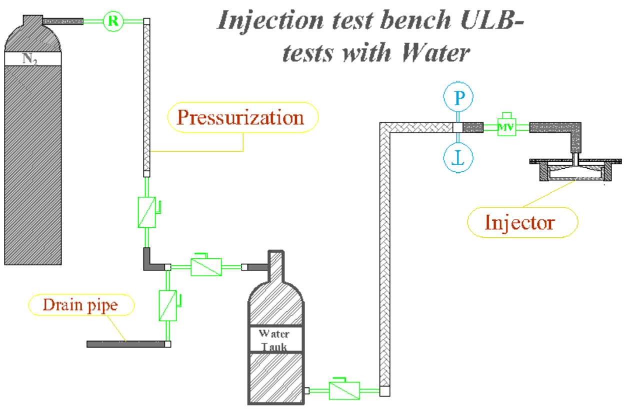


Figure 6: Cold flow tests bench

The discharge coefficient of the injectors was obtained using the set showed in the Figure (6). Here, to obtain the mass flow rate, the water tank was pressurized from 5 to 40 bar and the water weight difference was took by a scale with precision of 25 grams. To increase the precision of the measurement, each test was repeated 5 times for the same pressure level and injector configuration. Once that the geometrical characteristics of the injector were knew it was possible to evaluate the discharge coefficient, Eq. (3).
To measure the spray semi-angle ($\theta$) and visualize the liquid spray film it was used a Photon FASTCM SA4 high-speed camera with sample rate of 5000 frames per second. In this configuration, figure (7), two Samsung LED light source was used to obtain the best possible instantaneous picture and the scale in the black background is to help the post-test data analysis.

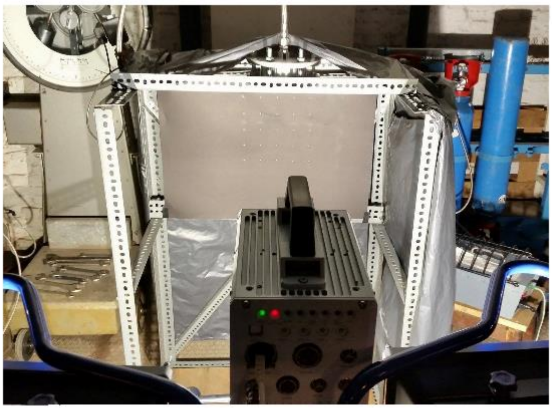

Figure 7: Installation of high-speed camera, light sources and injectors

The droplet size distribution of the spray and Sauter mean diameter (SMD) were acquired using a laser scattering (SMPATEC HELOS-VARIO/KR). Each measurement corresponds to three scans operations. The system is able to detect particles between 0.1 to 1750 µm. When the droplets go through the helium-neon laser beam (632.8 nm) the circular photodiode detector plate collects the laser scattered beam in angular sectors. Figure (8) shows one of the atomizer and the laser system. The central line of the laser beam was positioned on 70 mm under the exit of the injector's nozzle to fit with the length of the ULBHRE pre-chamber.

DOI: 10.13009/EUCASS2017-133



Figure 8: Atomizer coupled with the laser system

## 4. Experimental results

The aim of this work is to design, develop and test four different types of injector plates and to be apply in the injection system of the ULB lab-scale hybrid rocket motor (ULBHRE), using liquid nitrous oxide and paraffin as propellant. However, to reduce costs, it was used water in the first test campaign and after, when the both test benches were fully operational, we employed nitrous oxide ($N_2O$).

### 4.1 Showerhead injector (SH)

The showerhead injector (SH) is the most popular kind of injector plate and it has been applied in hybrid and liquid rocket engines over the years. Here, each element of the SH injector has 7 mm length and orifice diameter of 1.4 mm and it will be used as reference to evaluate the performance of the other types of injectors.
Figure (9) shows the flow pattern of the water in function of the pressure drop, in a range from 5 to 40 bar, where it is possible to notice the change in the flow before and after 25 bar. The Nitrous oxide behaviour at 45 bar is illustrated in the Figure (10) and, because of the fast expansion of the $N_2O$ at ambient temperature and pressure a clear separation between the liquid layer and the gas plume is not visible.
When we compare the water and Nitrous oxide flow pattern (figure 9-h and figure 10, respectively) it is possible to notice that an angle in the liquid $N_2O$ is formed in the exit of each injector orifice, in contrast to the water. The schematic in figure (11) illustrates this phenomenon.

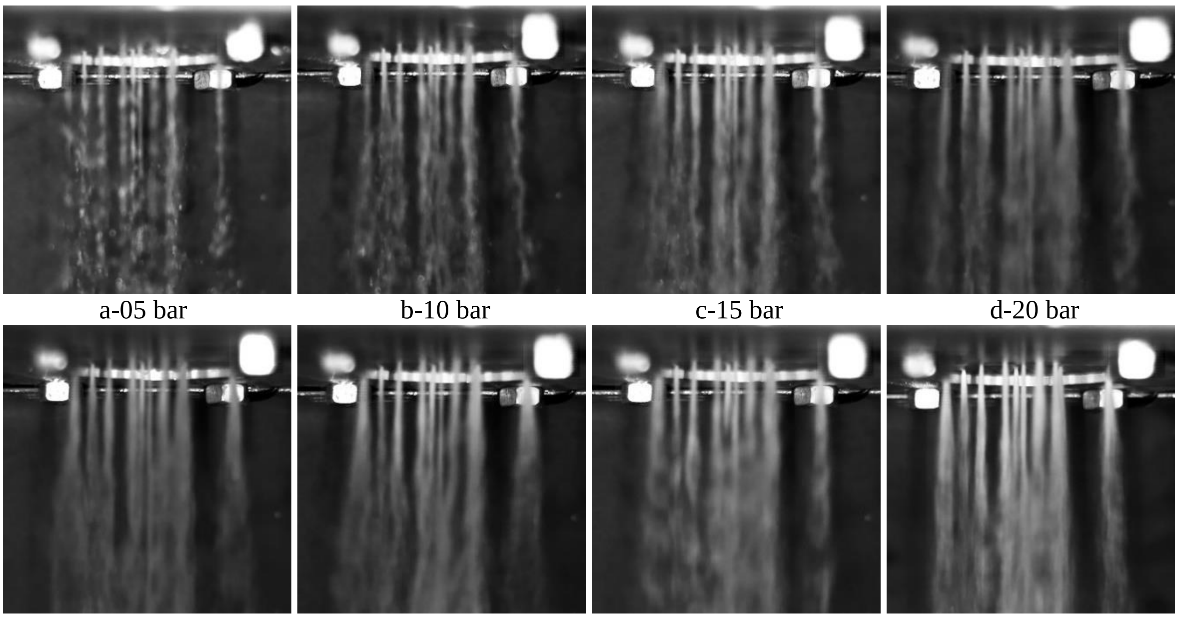

a-05 bar b-10 bar c-15 bar d-20 bar

e-25 bar f-30 bar g-35 bar h-40 bar

Figure 9: Showerhead injector water flow pattern – pressure from 5 to 40 bar

DOI: 10.13009/EUCASS2017-133



Figure 10: Showerhead injector using $N_2O$

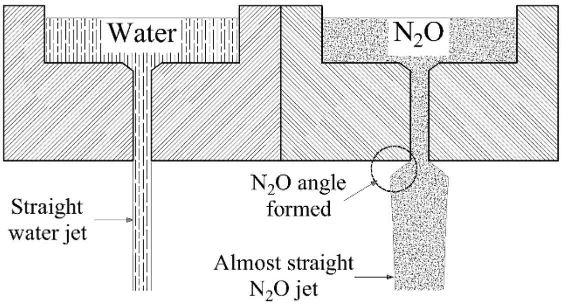


Figure 11: Schematic of water and $N_2O$ jet in SH injector

Figure (12) shows the experimental results for the mass flow rate in function of the pressure drop and figure (13) brings the comparison between the design and the experimental results for the discharge coefficient ($C_d$). The theoretical value for the $C_d$ was taken as 0.6 using references [10] and [22]. Both, the mass flow rate and the discharge coefficient consist of 5 individual measurements that we averaged.

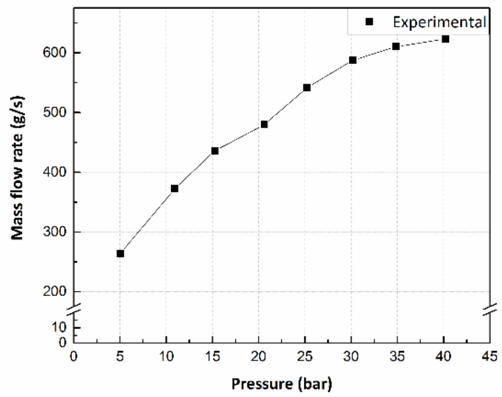


Figure 12: Mass flow rate using water as function of the pressure drop

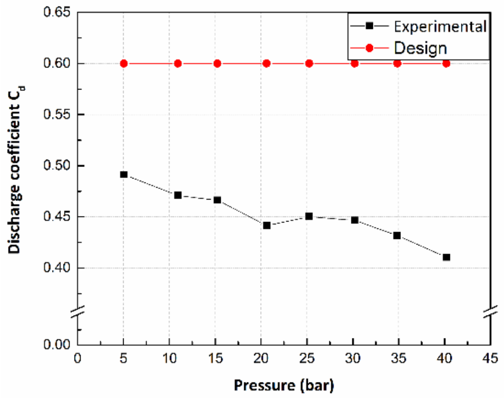


Figure 13: Discharge coefficient as function of the pressure drop

DOI: 10.13009/EUCASS2017-133



### 4.2 Hollow cone injector (HC)

Figure (14) shows the evolution of the water stream into Hollow Cone (HC) injector and the figure (15) presents the same configuration using liquid Nitrous Oxide. Despite to the fact that the external cone semi-angle ($\theta$) was defined as 15° during the design phase (figure 2), the flow pattern of both duty fluids is completely different. Using water, we observed a well-defined hollow cone and with the Nitrous oxide it is possible to notice the separation between the main liquid and the gas-liquid phase layer near the injector exit, and that at some point the liquid $N_2O$ flow becomes axial. In the second case, the spray semi-angle is not well delimited, but by the use of an image post-processing software and arbitrarily taking to account just the spray near the injector exit, we estimated the semi-angle as 45°.

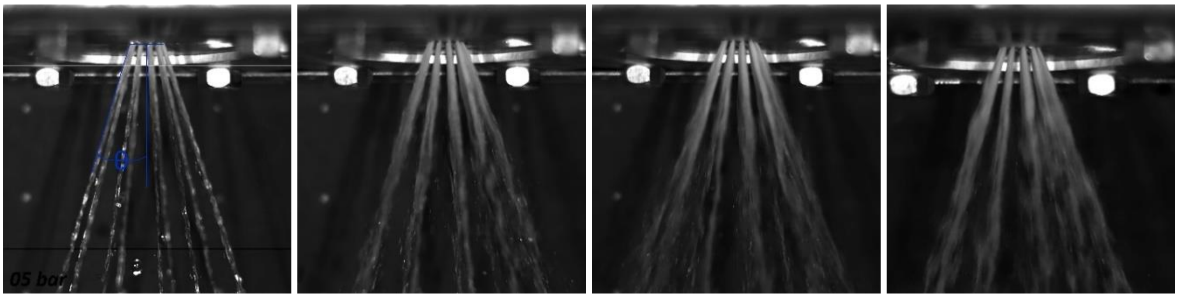


a-05 bar | b-10 bar | c-15 bar | d-20 bar

e-25 bar | f-30 bar | g-35 bar | h-40 bar

Figure 14: Hollow-cone injector water flow pattern – pressure from 5 to 40 bar

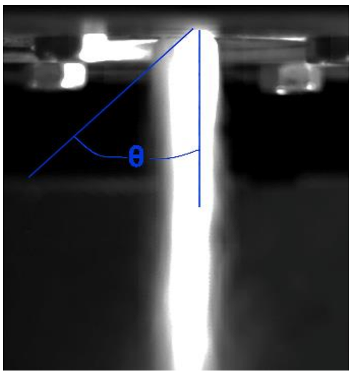


Figure 15: Liquid $N_2O$ discharged through hollow cone injector

Figures (16) and (17) show the experimental water mass flow rate and discharge coefficient of HC injector in terms of the injector pressure drop, respectively. The mass flow rate increase with increasing injector pressure differential and the slope of the curve decrease. Figure (17) brings the discharge coefficient experimental results and also its theoretical design phase value, 0.6. Generally, there are large similarities in the design of the HC and SH injectors as, equal same numbers of orifices with identical diameter and the same design discharge coefficient.

DOI: 10.13009/EUCASS2017-133



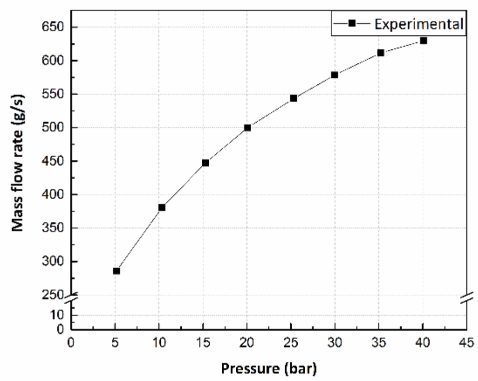


Figure 16: Water masse flow rate as function of injector pressure drop in the HC injector

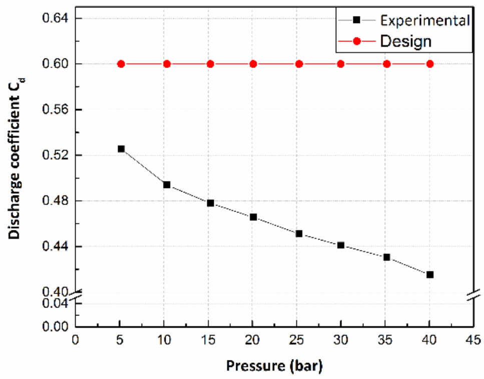


Figure 17: Discharge coefficient as function of injector pressure drop in the HC injector

### 4.3 Pressure swirl injector (PSW)

The pressure-swirl injector plate (PSW) designed to be use in the ULBHRE, it is composed of 6 individual PSW elements to deliver the same oxidizer mass flow rate. But, in order to perform the injector characterization at cold conditions it was used an individual PSW element set down in the centre of the PSW injector plate.

In order to see the influence of pressure on spray semi-angle, the pressure drop exercised is from 5 to 40 bar in steps of 5 bar. Each individual photograph was analysed using the commercial software AutoCad® and the reference points printed in the black background. The results are displayed in the table 3.

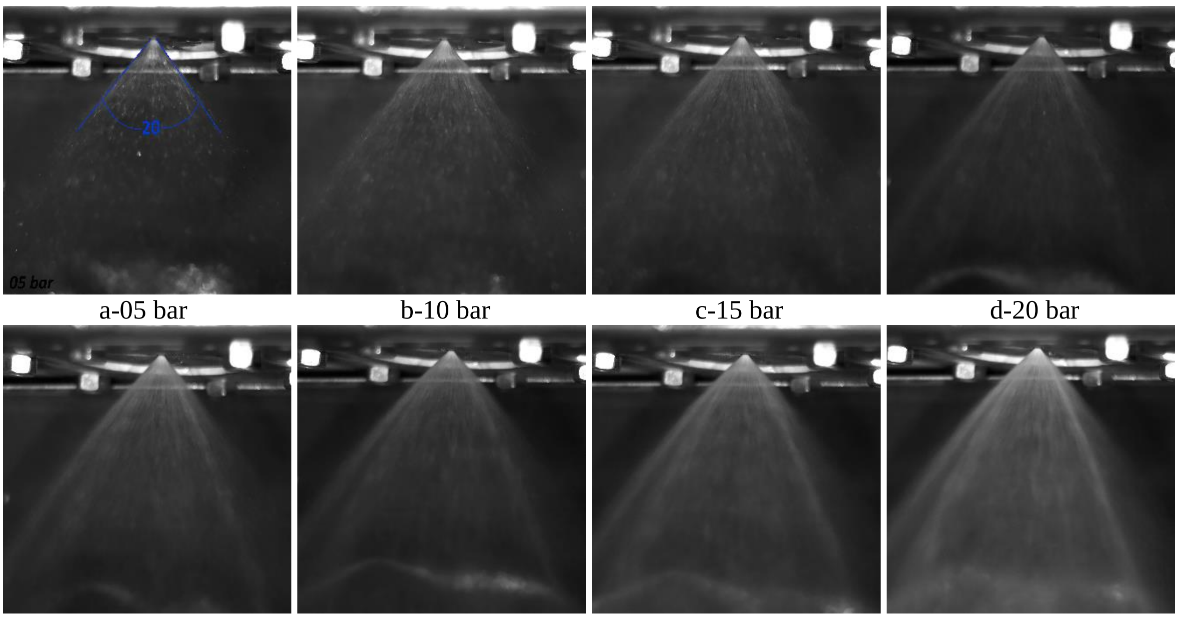


a-05 bar | b-10 bar | c-15 bar | d-20 bar

e-25 bar | f-30 bar | g-35 bar | h-40 bar

Figure 18: Water discharged through pressure swirl injector from 5 to 40 bar

DOI: 10.13009/EUCASS2017-133



Table 3: cone semi angle for water discharged by PSW atomizer

| **Difference of pressure (bar)** | **Experimental Semi-angle ($\theta$)** | **Difference of pressure (bar)** | **Experimental Semi-angle ($\theta$)** |
|---|---|---|---|
| 05 | 41 | 25 | 42.5 |
| 10 | 42 | 30 | 43 |
| 15 | 42.5 | 35 | 43 |
| 20 | 42.5 | 40 | 43 |

The semi-angle ($\theta$) can be estimated by the expression (7) developed by Giffen and Muraszew for a pressure-swirl atomizer (under ideal conditions) mentioned in [19].

$$\sin(\theta) = \frac{(\pi/2)\cdot C_d}{K\cdot(1+\sqrt{X})} \tag{7}$$

Where $K$ equal the atomizer constant $\frac{A_p}{D_s \cdot D_0}$, and $X$ is the ratio between the air core area ($A_a$) and the nozzle orifice exit area ($A_0$). The diameter of the core area is the discharge diameter ($D_0$) removing the sheet thickness ($t$), which it was estimated by the equation (8) given by Rizk and Lefebvre [14].

$$t = 3.66 \left[\frac{D_0 \cdot FN \cdot \mu}{(\rho \cdot \Delta P)^{0.5}}\right]^{0.25} \tag{8}$$

The spray semi angles ($\theta$) were calculated using $C_d$ design and $C_d$ estimated in equation (6) developed by Jones. Figure (19) shows the difference between both theoretical $\theta$ and brings the experimental $\theta$ also, they evaluated as function of the pressure drop. When the $\Delta P$ increases, the experimental spray semi-angles barely change, just 2° difference between the angle obtained at 40 bar and the angle achieved with 5 bar. However, both theoretical angles decrease a little bit. In figure (19) we notice also that the experimental $\theta$ is really close, in high pressure up than 30 bar, to the theoretical one calculated using $C_d$ of Jones.

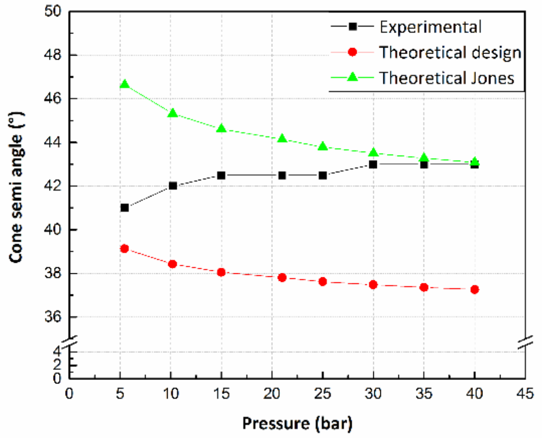


Figure 19: Spray semi-angle of PSW atomizer as function of the injector pressure drop

Figure (20) shows the liquid nitrous oxide passed through PSW atomizer. The spray semi-angle obtained in this case (55.5°), also arbitrarily taking in to account just the spray near the injector exit, is greater when compared with the water results, around 43° (table 3). But, the cone is not perfectly formed once that after the injector exit we have a liquid-gas $N_2O$ flow. In addition, the viscosity of nitrous oxide is lower than the water, and the viscosity affects in the spray semi-angle, which decreases with increasing liquid viscosity [15].

DOI: 10.13009/EUCASS2017-133



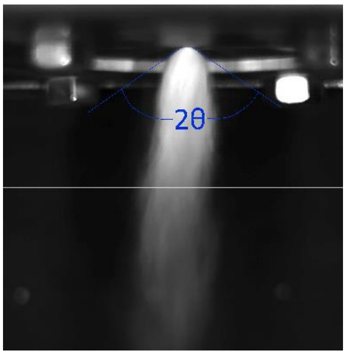


Figure 20: Liquid $N_2O$ discharged through pressure swirl injector

Figure (21) illustrates the variation of water mass flow rate. The experimental values of discharge coefficient are presented in figure (22) accompanied by $C_d$ design, $C_d$ calculated by equations (5) and (6) given by Rizk and Lefebvre [14] and Jones [20], respectively.

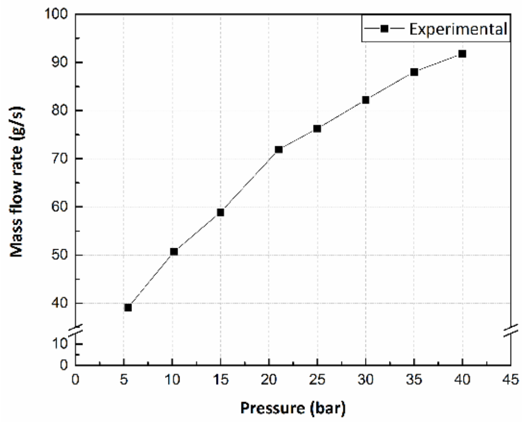


Figure 21: Water masse flow rate as function of injector pressure drop in the PSW injector

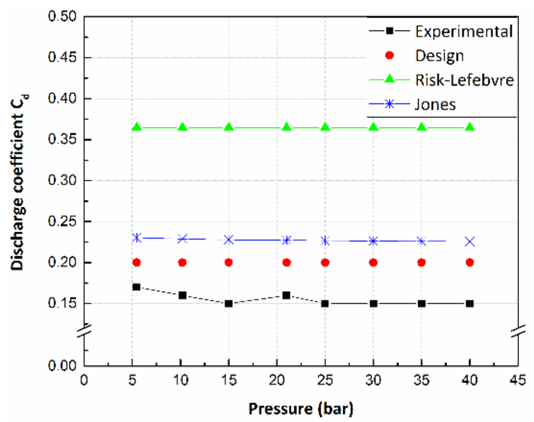


Figure 22: Discharge coefficient as function of injector pressure drop in the PSW injector

The measured SMD is presented in figure (23) and the density distribution in the figure (24). The Sauter Mean Diameter reduces when the pressure drop increases, and it has reached 40.71 µm for a pressure drop equal to 40 bar. These results show a good agreement with the literature [13].

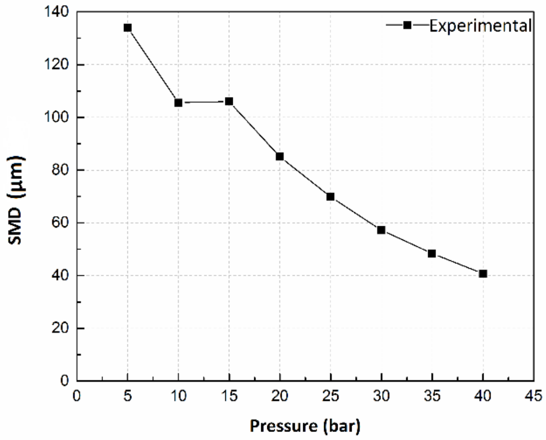


Figure 23: Experimental SMD vs injector pressure differential in PSW atomizer

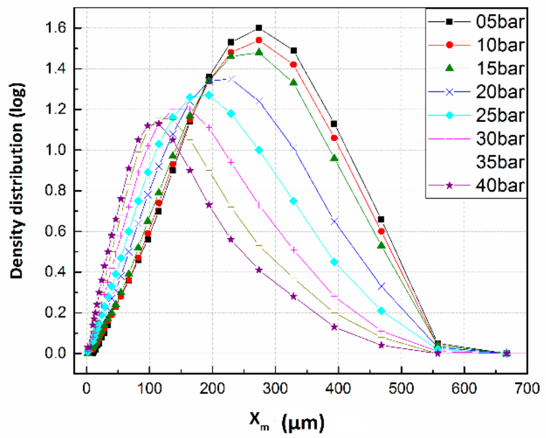


Figure 24: Density distribution

### 4.4 Vortex injector (VOR)

Radial axial injection, VOR, is composed by 6 orifices with 45° degrees of inclination from the injector plane. Figure (25) shows the evolution of water flow with injector pressure difference from 5 to 30 bar, and it is possible to notice that after 30 bar there is no visible difference between the photographs. The results with Nitrous oxide are presented on figure (26).

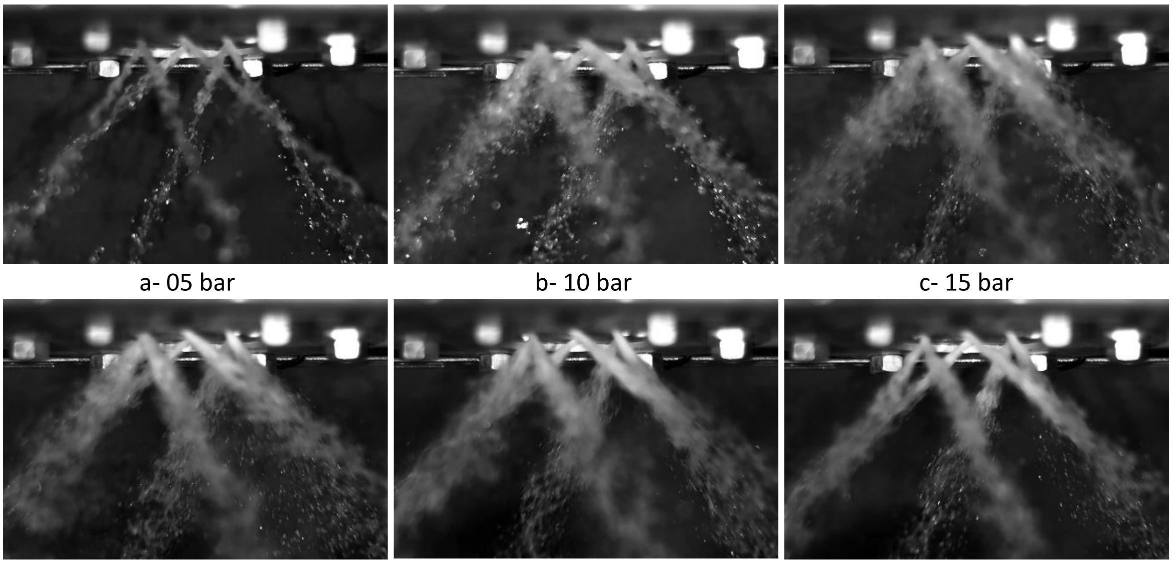

a- 05 bar b- 10 bar c- 15 bar

d- 20 bar e- 25 bar f- 30 bar

Figure 25: Water discharged through vortex injector from 5 to 35 bar using HSC

DOI: 10.13009/EUCASS2017-133



Figure 26: Liquid $N_2O$ discharged through vortex injector

Figures (27) and (28) show the evolution of water mass flow rate and discharge coefficient in function of the pressure drop in vortex injector, respectively, where it is possible to see that the mass flow rate increases almost linear with increasing pressure drop. The experimental values of the discharge coefficient started to decrease with increasing the pressure drop until 30 bar, after, it stabilized at a value equal to 0.21.

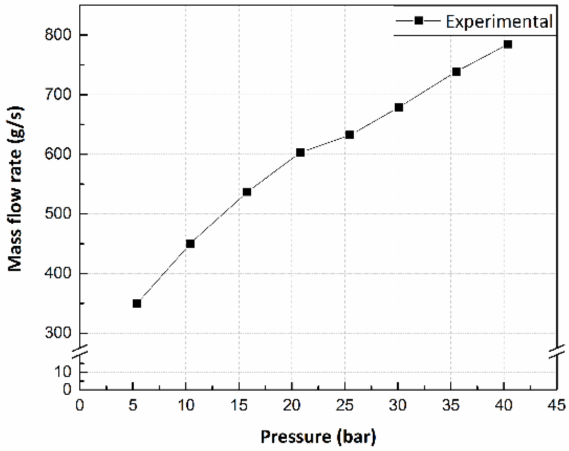


Figure 26: Water masse flow rate as function of injector pressure drop in VOR injector

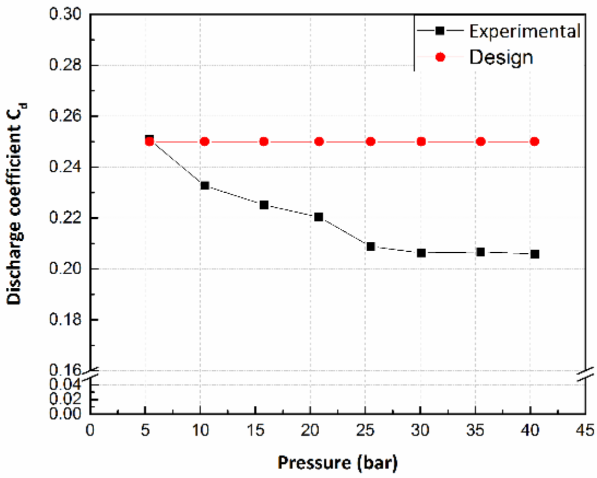


Figure 27: Discharge coefficient as function of injector pressure drop in VOR injector

## 4. Conclusions

This work presents the design and the characterization at cold flow conditions of four different types of injectors, namely showerhead (SH), hollow-cone (HC), pressure-swirl (PSW) and vortex atomizer (VOR), to be applied in the ULB lab-scale hybrid rocket motor (ULBHRE). The ULBHRE motor was designed to use nitrous oxide and paraffin as propellant.
For this purpose, a new test bench was assembled in the Aero-Thermo-Mechanics Department with the support of the Royal Military Academy of Belgium (RMA) and the collaboration of the University of Brasília.

DOI: 10.13009/EUCASS2017-133



The first analysis performed was the study of the flow pattern by the use of a high-speed camera with sample rate of 5000 fps. In this case, we notice a considerable discrepancy between the results using water and nitrous oxide as duty fluid, mainly with the PSW and the HC injectors. But, using SH and VOR the stream profile with water are closer than with $N_2O$.

However, the use of the water to obtain the discharge coefficient provides very accurate results. The injectors which the pressure has higher influence over the discharge coefficient were the HC and SH and the lower was the PSW and VOR.

A more detailed analysis was carried out with the pressure-swirl atomizer in order to estimate the spray-semi angle and the Sauter Mean Diameter. The results with water give us the values of 43° and 40.71 µm at 40 bar, respectively. Using the laser scattering we also obtained the droplet size distribution of the spray, figure (24). In spite of the fact that the values of the spray semi-angle, SMD and the droplet size distribution also showed good agreement with the literature [13], these results for the Nitrous oxide were inconclusive due to the optical concentration in the laser detector.

Based on these results the future works are: (i) development of a methodology to reduce the optical concentration to obtain the SMD and the drop size distribution using also nitrous oxide and (ii) carry out the fire test with the ULBHRE to evaluate the performance of each individual injector over the fuel regression rate and combustion stability.

## Acknowledgements

M. Bouziane greatly acknowledge the Algerian Ministry of Defence for the scholarship of his PhD student position in the RMA. Mr A. E. M. Bertoldi would like to express his thanks to the Brazilian National Council for Scientific and Technological Development (CNPq) for the split-site doctoral scholarship, and the authors thanks the technicians of Aero-Thermo-Mechanics at ULB and chemical department at RMA for their helps.

## References

[1] Knuth, W., Gramer, D., Chiaverini, M., & Sauer, J. (1998). Development and testing of a vortex-driven, high-regression rate hybrid rocket engine. In 34th AIAA/ASME/SAE/ASEE Joint Propulsion Conference and Exhibit (p. 3507).

[2] Knuth, W., Chiaverini, M., Gramer, D., & Sauer, J. (1998). Experimental investigation of a vortex-driven high-regression rate hybrid rocket engine. In *34th AIAA/ASME/SAE/ASEE Joint Propulsion Conference and Exhibit* (p. 3348).

[3] Knuth, W., Gramer, D., Chiaverini, M., Sauer, J., Whitesides, R., & Dill, R. (1998, July). Preliminary CFD analysis of the vortex hybrid rocket chamber and nozzle flow field. In *34th AIAA/ASME/SAE/ASEE Joint Propulsion Conference and Exhibit* (p. 3351).

[4] Knuth, W. H., Chiaverini, M. J., Sauer, J. A., & Gramer, D. J. (2002). Solid-fuel regression rate behavior of vortex hybrid rocket engines. *Journal of Propulsion and power*, *18*(3), 600-609.

[5] Yuasa, S., Shimada, O., Imamura, T., Tamura, T., & Yamoto, K. (1999). A technique for improving the performance of hybrid rocket engines. In *35th Joint Propulsion Conference and Exhibit* (p. 2322).

[6] Saburo, Y., Noriko, S., & Kousuke, H. (2012). Controlling Parameters for Fuel Regression Rate of Swirling-oxidizer-flow-type Hybrid Rocket Engine. In *48th AIAA/ASME/SAE/ASEE Joint Propulsion Conference & Exhibit* (p. 4106).

[7] Yuasa, S., Yamamoto, K., Hachiya, H., Kitagawa, K., & Oowada, Y. (2001). Development of a small sounding hybrid rocket with a swirling-oxidizer-type engine. In *37th Joint Propulsion Conference and Exhibit* (p. 3537).

[8] Takashi, T., Yuasa, S., & Yamamoto, K. (1999). Effects of swirling oxidizer flow on fuel regression rate of hybrid rockets. In *35th Joint Propulsion Conference and Exhibit* (p. 2323).

[9] Bellomo, N., Barato, F., Faenza, M., Lazzarin, M., Bettella, A., & Pavarin, D. (2011, August). Numerical and experimental investigation on vortex injection in hybrid rocket motors. In *47th AIAA/ASME/SAE/ASEE Joint Propulsion Conference & Exhibit* (p. 5675).

[10] Bellomo, N., Faenza, M., Barato, F., Bettella, A., Pavarin, D., & Selmo, A. (2012). The" Vortex Reloaded" project: experimental investigation on fully tangential vortex injection in $N_2O$-paraffin hybrid motors. In *48th AIAA/ASME/SAE/ASEE Joint Propulsion Conference & Exhibit* (p. 4304).

[11] Bellomo, N., Faenza, M., Barato, F., Bettella, A., & Pavarin, D. (2012). The" Vortex Reloaded" project: numerical investigation on fully tangential vortex injection in $N_2O$-paraffin hybrid motors. In *48th AIAA/ASME/SAE/ASEE Joint Propulsion Conference & Exhibit* (p. 3903).

[12] Messineo, J., Lestrade, J. Y., Hijlkema, J., & Anthoine, J. (2016, May). 3D miles simulation of a hybrid rocket with SWIRL injection. In *Space Propulsion 2016*.

DOI: 10.13009/EUCASS2017-133




[13] Lacava, P. T., Bastos-Neto, D., Pimenta, A. P., 2004. Design Procedure and Experimental Evaluation of Pressure-Swirl Atomizers. *In: 24th International Congresso of the Aeronautical Sciences,* ICAS.

[14] Rizk, N. K., & Lefebvre, A. H. (1985). Internal flow characteristics of simplex swirl atomizers. *Journal of Propulsion and Power*, *1*(3), 193-199.

[15] Lefebvre, A. H., & Ortman, J. (1985). Fuel distributions from pressure-swirl atomizers. *Journal of Propulsion and Power*, *1*(1), 11-15.

[16] Chen, S. K., Lefebvre, A. H., & Rollbuhler, J. (1992). Factors influencing the effective spray cone angle of pressure-swirl atomizers. *Journal of Engineering for gas turbines and power*, *114*(1), 97-103.

[17] Lefebvre, A. H., & Wang, X. F. (1987). Mean drop sizes from pressure-swirl nozzles. *Journal of propulsion and power*, *3*(1), 11-18.

[18] Carmicino, C., & Sorge, A. R. (2006). Influence of a conical axial injector on hybrid rocket performance. *Journal of Propulsion and Power*, *22*(5), 984-995.

[19] Silva Couto, H., Lacava, P. T., Bastos-Netto, D., & Pimenta, A. P. (2009). Experimental Evaluation of a Low Pressure-Swirl Atomizer Applied Engineering Design Procedure. *Journal of propulsion and power*, *25*(2), 358-364.

[20] Jones, A. R., design optimization of a large pressure jet atomizer for power plant. *Proceedings of the 2nd International Conference on Liquid Atomization and Spray Systems, Hemisphere, New York, page 181–185,* 1982.

[21] Lefebvre, A. H., Atomization and Sprays, Hemisphere, New York,1989.

[22] Sutton, G. P., & Biblarz, O. (2016). *Rocket propulsion elements*. John Wiley & Sons.